Chapter 2
Experimental and Computational Investigation of Out-of-Plane Low Velocity Impact Behavior of CFRP Composite Plates

O.T. Topac, B. Tasdemir, B. Gozluklu, E. Gurses, and D. Coker

Abstract Strength of composite materials under transverse loading has remained a major weakness despite numerous advancements in composite technologies. Most frequent and critical result of this characteristic is internal delamination damage, which is undetectable and lead to major strength reduction in the structure. This condition is usually encountered in low-velocity impact situations which frequently occur during the maintenance of aircraft. Past studies have successfully developed experimental and analysis methods for accurately predicting impact force history and damage footprint based on the comparison with post-impact results. However, there is almost no experimental work on the progression sequence of damage during impact in the literature. This paper focuses on experimental and computational investigation of the damage initiation and growth process during low-velocity impact of $[0_7/90_4]_s$ and $[90_7/0_4]_s$ cross-ply CFRP laminates. In the experiments, through-the-thickness direction is tracked using ultra-high speed camera and DIC technique to record damage progression and dynamic strain fields. In the numerical part of the study 3-D explicit, finite element analysis is conducted to model matrix crack initiation and propagation. The finite element results are then compared with experiments in terms of failure modes and sequence.

Keywords Delamination • Matrix cracking • Transverse impact • High-speed camera • Experimental validation

2.1 Introduction

Due to the advances in composite technologies, carbon-fiber reinforced polymer (CFRP) composite laminates are widely used in a large variety of engineering applications. Specifically, in aerospace industry, composite material application has increased up to 500 % in the past 20 years [1]. In spite of greater strength of composites, they are much weaker under loading in through-the-thickness (transverse) direction. This results in a sudden and catastrophic brittle failure. This kind of loading is encountered in impact situations, which frequently occur during ground operations and maintenance of aircraft. Among impact conditions with different velocities, low-velocity impact (LVI) has a special importance since it creates insidious delamination damage inside the laminate. It occurs frequently and usually without any visible damage from the outside of structure. Hence, they can stay unrepaired for the remaining life of the aircraft. In aerospace industry, this phenomenon is considered as one of the most critical weaknesses of composite materials. For damage tolerant design, element level LVI tests are generally relied upon, which usually requires hundreds of specimens for different test and specimen configurations. However, it is impossible to conduct impact tests for each condition. Due to the abundant requirement of tests and uncertainty of the process, the designed damage tolerant structures are generally thicker and heavier than required.

O.T. Topac
Department of Aerospace Engineering, Middle East Technical University, Ankara 06800, Turkey

Helicopter Group, Turkish Aerospace Industries, Ankara 06980, Turkey
e-mail: tanaytopac@gmail.com

B. Tasdemir • E. Gurses
Department of Aerospace Engineering, Middle East Technical University, Ankara 06800, Turkey

B. Gozluklu
Helicopter Group, Turkish Aerospace Industries, Ankara 06980, Turkey

D. Coker (✉)
Department of Aerospace Engineering, Middle East Technical University, Ankara 06800, Turkey

METU Center for Wind Energy, Middle East Technical University, Ankara 06800, Turkey
e-mail: coker@metu.edu.tr

A.M. Beese et al. (eds.), *Fracture, Fatigue, Failure and Damage Evolution, Volume 8*, Conference Proceedings of the Society for Experimental Mechanics Series, DOI 10.1007/978-3-319-21611-9_2

In the literature, low-velocity impact response of composite laminates is investigated in terms of load and displacement histories of the laminate and resulting damages. One of the pioneering low velocity impact experiments on laminated composites was conducted by Cantwell et al. where the mass was dropped from a simple drop-weight tower and resulting damage was successfully observed by non-destructive inspections [2]. In their experimental and numerical study, Choi et al. investigated impact-induced damage mechanisms [3]. Beam-like 2D composite plates with several cross-ply stacking sequences were impacted by 2D impactors to achieve a damage scheme uniform in width direction. Resulting damages obtained for $[0_n/90_m/0_n]$ and $[0_n/90_m/0_n/90_m/0_n]$ laminates showed coupled matrix cracking and delamination, the characteristic impact-induced damage. In a computational effort, a finite element analysis of a simple 2D [0/90/0] beam done where matrix cracking and delamination damage interaction were simulated [4]. More recently, effects of dispersed stacking sequence were investigated in a combined experimental and numerical study, in which element level impact experiments were conducted on composite laminates according to ASTM D7136 standards. In numerical side, finite element analyses were conducted with matrix, fiber and delamination damage considerations to completely simulate experiments [5, 6]. A good agreement was obtained for post-impact results of experiments and analyses in terms of resulting damage, force, displacement and energy histories. However, to this date, almost no effort has been made to get a complete understanding and computational analysis of matrix and delamination damage progression sequence under impact conditions.

This study aims to observe damage progression sequence in carbon-epoxy composite laminated plates and verify the damage modeling of finite element analyses (FEA). Low velocity impact experiments are conducted on two types of [0/90] cross-ply specimens. Resulting matrix cracking and delamination process is captured by a high speed camera (1M fps). In computations, the experiment conditions are simulated in ABAQUS/Explicit and matrix damage evolution is investigated. In those, intralaminar matrix cracking damage is modeled via continuum damage mechanics (CDM) based failure approach proposed by Christensen [7] and compared with real-time results from high-speed camera.

2.2 Experimental Method

2.2.1 Experimental Setup

The experimental setup consists of an external structure for drop weight-tower, a base fixture to clamp the composite specimen and a guiding rail to provide an aimed drop of the impactor. CAD drawing and photograph of the setup with high speed camera and lighting are shown in Fig. 2.1. At the base fixture, both ends of the test specimen are fixed between two thick aluminum plates. In order to prevent possible sliding, the specimen is drilled and bolted from its ends to the base structure. Guiding rail is provided by a hollow aluminum tube with a rectangular cross-section vertically fixed above the center of the specimen.

Impact specimens, are made of Cytec T300/895 CFRP material with individual ply thickness of 0.16 mm. The size of the specimen is 85 mm × 15 mm which provides plane strain condition. Two different stacking sequences of $[0_7/90_4]_s$ and $[90_7/0_4]_s$ are manufactured where the thickness of the specimens are equal to 3.5 mm. The impactor, seen in Fig. 2.2a, is made of SAE 304 stainless steel material and designed to have variable mass of 0.365, 0.788 and 1.21 kg. It is designed with semi-cylindrical cross section to create line load impact conditions in the width direction of the specimen. The progression of damage during impact event is captured by Photron SA5 high speed camera, capable of capturing images at rates up to one million frame per second (fps).

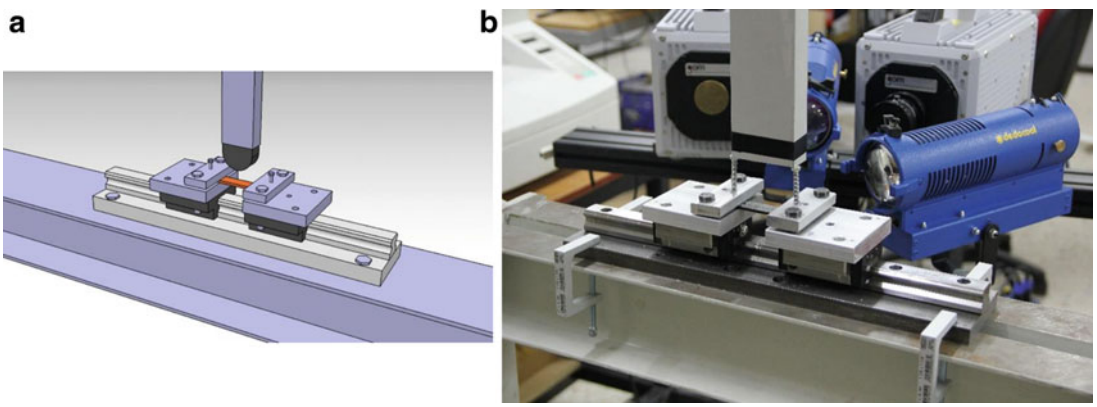

Fig. 2.1 Experimental set-up for line load impact testing; (**a**) CAD drawing and (**b**) photograph of setup with high speed camera and lighting

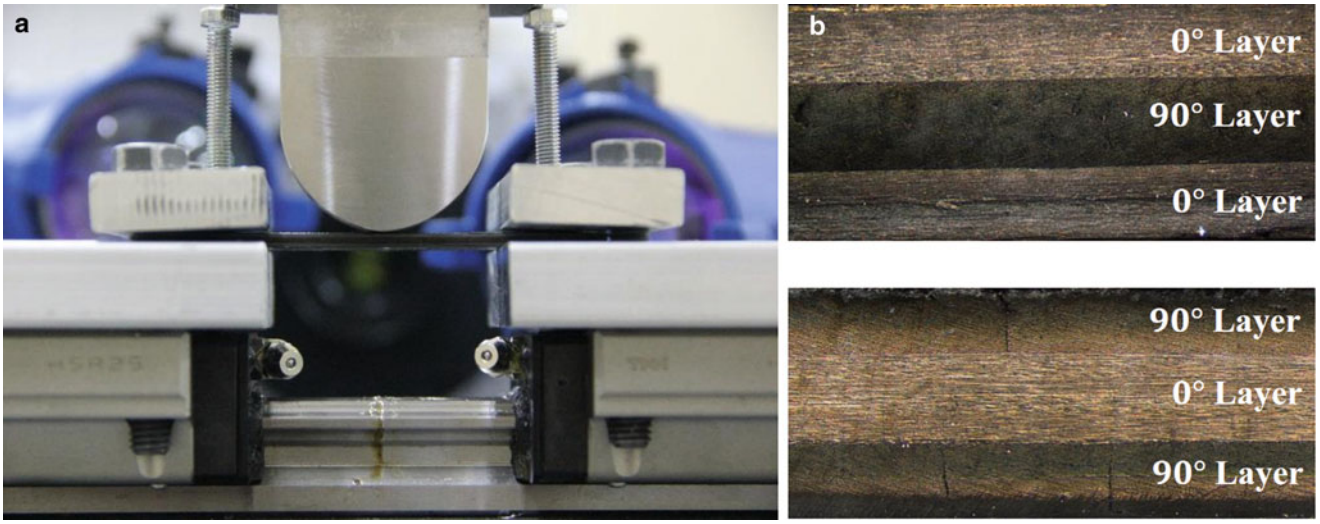

Fig. 2.2 (**a**) Close-up side-view of the specimen with the impactor and grips, (**b**) micrograph images of two stacking sequences used in this paper: $[0_7/90_4]_s$ and $[90_7/0_4]_s$

2.2.2 Experimental Procedure

Firstly, side sections of composite specimens are polished by Minitech-233 polishing machine in order to achieve clear visualization of their side section. Before conducting the tests, polished specimens were scanned with Huvitz HDS-5800 Digital Microscope from the edge section to reveal manufacturing flaws which were in the acceptable limits. Images are captured with lens having zoom rate of 50×.

The experiments are conducted as drop-weight impact events. Two sets of specimens with different stacking sequences are tested, each set having four individual composite beams. The high-speed camera is focused on at the edge section of the composite with frame rates from 15,000 to 210,000 fps are used to provide adequate compromise between capture rate of crack progression and picture resolution. Steel impactor of 0.365 kg is symmetrically placed inside the guiding rail and dropped from 1 m height resulting in 3.58 J kinetic energy at the instant of impact.

A free fall of impactor is assumed and friction between impactor and guiding rail is neglected in analyses and evaluation of tests. Image acquisition module of high-speed camera is triggered just before impact and the whole impact event is successfully captured. After first impact, bounce-back of the impactor is prevented to avoid any further damage after the first contact. An illustrative picture just before impact is given in Fig. 2.2a. After the experiments, resulting damage scheme is optically examined with microscope.

2.3 Computational Method

In the computational part of this study, simplified experimental impact case is modeled as seen in Fig. 2.3 and simulated in ABAQUS/Explicit finite element software. For the geometrical model, only the region of laminate between gripping tabs is modeled which results in a 45 × 15 mm plate. Rest of the plate beyond the tabs is lumped in the clamped boundary conditions. Material properties of T300/985 carbon/epoxy composite are obtained from manufacturer specification sheet and previous studies [8, 9] which are provided in Table 2.1. The impactor is modeled as an analytical rigid body with lumped mass of 0.365 kg at its centroid. An initial vertical velocity of 4.3 m/s that corresponds to a free fall from 1 m is defined for the impactor.

In computational analysis, only matrix cracking damage is considered and compared with experiments. The composite laminate is meshed with solid C3D8R (Reduced integration, eight noded hexagonal) elements as in Fig. 2.3 where each layer is modeled with one element in thickness direction, and in longer side of the beam, elements are biased to have a finer mesh near the impacting region. The total number of elements is 580,800. Contact condition between impactor and composite laminate is defined with general contact algorithm of ABAQUS. Normal behavior is defined as hard contact with penalty algorithm and tangential Coulomb friction between impactor and composite is defined with a friction coefficient of $\mu = 0.3$ based on the study of [6, 10].

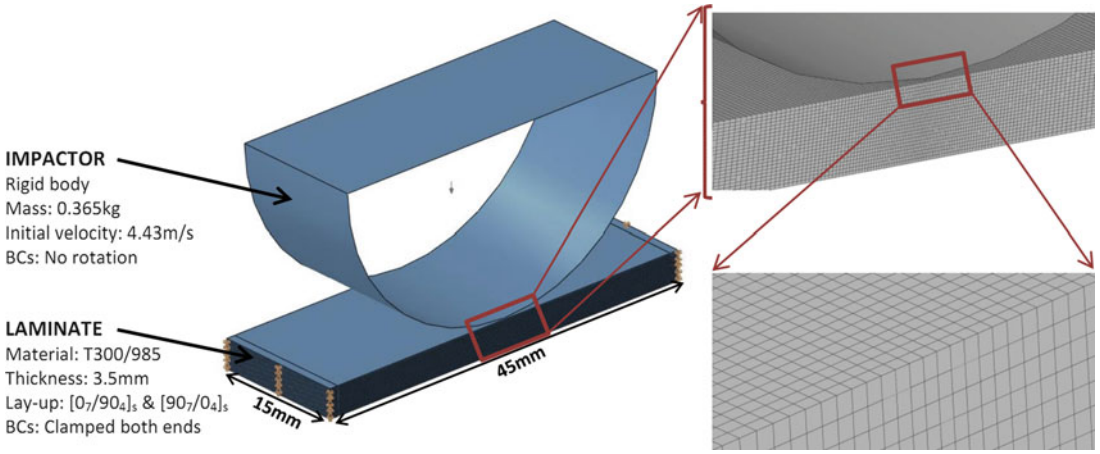

Fig. 2.3 Finite element model and mesh of the impact analysis

Table 2.1 Cytec T300/985 ply properties

Density	1600 kg/m^3
Elastic properties	$E1 = 106$ GPa; $E2 = E3 = 7.8$ GPa; $\nu_{12} = \nu_{13} = 0.30$; $\nu_{23} = 0.44$; $G_{12} = G_{13} = 10.5$ GPa; $G_{23} = 2.7$ GPa
Strength properties	$S_{22}^{+} = 50$ MPa; $S_{22}^{-} = 170$ MPa; $S_{12} = 170$ MPa; $S_{13} = S_{23} = 95$ MPa

In computational analysis, only matrix cracking damage is considered and compared with experiments. Intraply damage in composite materials is commonly studied by continuum damage mechanics (CDM), where several load interaction criteria exist to predict initiation of crack under normal and shear loading of the plies. In this study, Christensen CDM criterion with only matrix cracking consideration is applied using Autodesk Simulation Composite Analysis 2015 plugin. Christensen failure criterion is chosen due to its high order transverse stress terms ($\sigma_{33}^{m}, \sigma_{13}^{m}, \sigma_{23}^{m}$) in crack prediction, which are dominant in transverse impact situations. Christensen criterion considers tensile and compressive failure strengths of a ply in normal orthotropic directions $\left(S_{11}^{+}, S_{11}^{-}, S_{22}^{+}, S_{22}^{-}\right)$ and absolute values of longitudinal and transverse shear strengths (S_{12}, S_{23}). It assumes that matrix crack initiates when the interaction equation becomes equal to or greater than one:

$$\left(\frac{1}{S_{22}^{+}} - \frac{1}{S_{22}^{-}}\right)(\sigma_{22} + \sigma_{33}) + \frac{1}{S_{22}^{+} S_{22}^{-}}(\sigma_{22} + \sigma_{33})^2 + \frac{1}{S_{23}^{2}}\left(\sigma_{23}^{2} + \sigma_{22}\sigma_{33}\right) + \frac{1}{S_{12}^{2}}\left(\sigma_{12}^{2} + \sigma_{13}^{2}\right) \geq 1$$

2.4 Results

2.4.1 Experimental Results

2.4.1.1 Impact Testing of $[0_7 / 90_4]_s$ Unidirectional CFRP Laminates

Series of photographs are taken with high speed camera from the side of the specimen. While observable damage occurred at the side section, no visible damage is produced on the contact region between impactor and the specimen. In the results, 0 μs represents the impact instant. In Fig. 2.4, series of high speed camera images taken at 15,000 fps, 66.7 μs interframe time are presented. The photograph in Fig. 2.4a shows the impactor and specimen just before impact and Fig. 2.4b, taken 133 μs later, shows loading of the composite plate with no visible sign of damage. One frame later, shown in Fig. 2.4c complete composite failure is observed. Resulting damage scheme closely resembles the results of Choi et al. on a similar composite laminate [3]. Delaminations between the 0° and 90° plies are observed consisting of a delamination of the upper interface under the impactor and a delamination of the lower interface away from the impact region. Matrix cracks appear in the 90° plies connecting the two delaminations. However, damage progression and its sequence are not captured at this camera speed.

The micrograph images of the front and mirrored back faces of the laminate after the experiment are shown in Fig. 2.5a and b, respectively. The delamination and the matrix cracking patterns are observed to be the same throughout the width of the specimen.

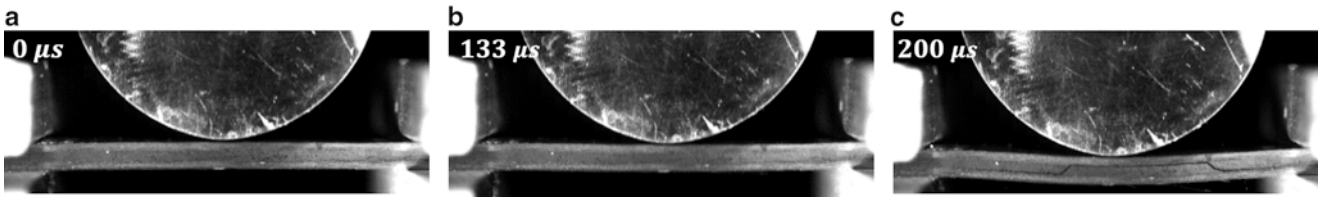

Fig. 2.4 High speed camera images of $[0_7/90_4]_s$ specimen taken at 15,000 fps. (**a**) Just before the impact and (**b**) after impact subjected to loading with no damage, (**c**) after damage initiation

Fig. 2.5 Micrograph images of two faces of damaged specimen showing uniformity of damage

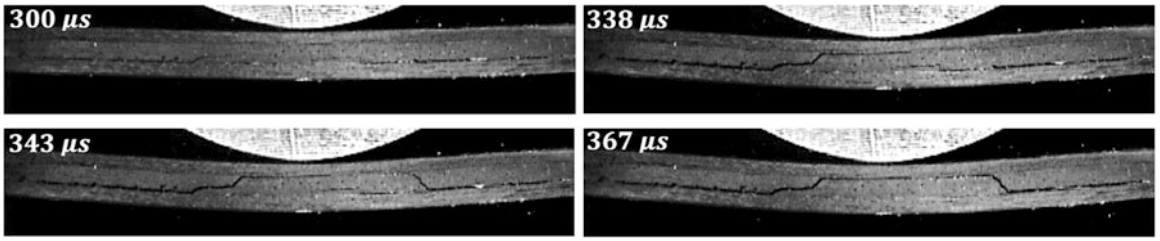

Fig. 2.6 High speed camera images of $[0_7/90_4]_s$ specimen taken at 210,000 fps showing progression of matrix cracking and delamination

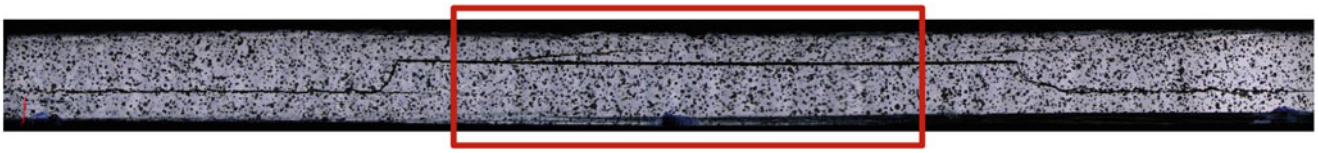

Fig. 2.7 Micrograph of laminate after the impact experiment showing the final failure pattern and the location of the field of view of the high speed camera

To look at the failure sequence at a higher time resolution, an impact test was conducted under the same conditions and the results were captured with the high speed camera at 210,000 fps, 4.76 μs interframe time. In the first frame the composite is loaded and initial delamination in the bottom 0/90 interface can be seen. 38 μs later a matrix crack starts from the lower interface and is followed by a delamination at the upper interface growing towards the impact point. Five microseconds 5 μs later, a second matrix crack initiates at the right hand side from the bottom interface and propagates towards the upper interface. In the last picture, 24 μs later, upper delamination grows from the matrix crack towards the impact point and joins with the upper left delamination front. This illustrates the failure sequence of $[0_7/90_4]_s$ laminates under low velocity impact (Fig. 2.6).

In order to observe the strain fields at the crack front during impact, DIC analysis is performed on the high speed camera images captured at 20,000 fps. The post-impact micrograph is shown in Fig. 2.7 with the final failure pattern similar to the previous cases. Because of the resolution, framing rate and shutter speed limitations, the field of view of the high speed camera is limited to the area just under the impact site, highlighted with red frame in Fig. 2.7. The high speed camera pictures and the Tresca strain fields using DIC method during the impact event are shown in Fig. 2.8a and b, respectively. At 100 μs, initial delamination fronts are observed at upper interface from both sides and lower interface from only the left side. One frame (50 μs) later, the delaminations at the upper interface propagate towards the center from both sides, however the lower delamination is found to have arrested. In the final frame, the upper delaminations from both sides combine to form a single

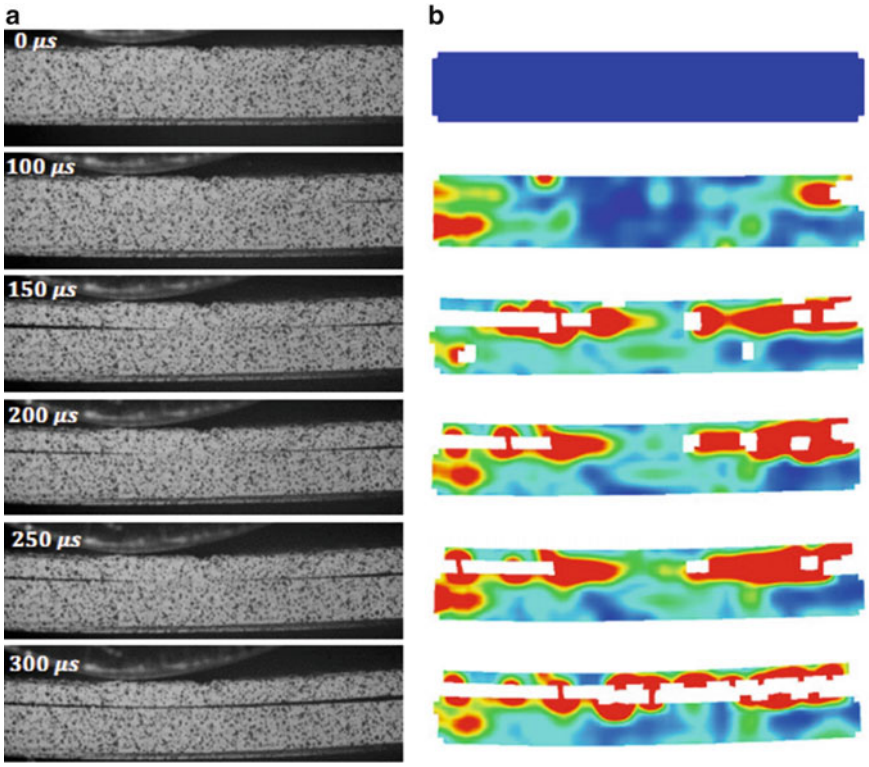

Fig. 2.8 Close-up of the middle section of $[0_7/90_4]_s$ specimen showing stress fields at lower and upper delamination regions. (**a**) High speed camera images, (**b**) Tresca strain contours from Digital Image Correlation (DIC) analysis program ARAMIS

upper delamination. An interesting observation is that between 150 and 250 μs, the delaminations seem to arrest and even show closure of delamination front. However, upon closer examination, the crack surfaces, which have coalesced at 150 μs, are observed to close due to compressive waves from the impactor. At 300 μs, the tensile waves arrive and the delamination opens up.

2.4.1.2 Impact Testing of Unidirectional OE $[90_7 / 0_4]_s$ CFRP Laminates

Second set of impact tests are conducted on $[90_7 / 0_4]_s$ unidirectional CFRP laminates. The images during the impact event were captured at 20,000 fps for DIC analysis; however due to shutter speed limitations blurry images were obtained and could not be processed for DIC. The images of the plate at 0, 200, 300 and 700 μs after impact are shown in Fig. 2.9. At 200 μs crack is initiated from the middle lower layer because of normal tensile stresses on matrix material caused by bending of the beam. Two frames later, at 300 μs, four additional matrix cracks are observed next to other cracks with an average of 3.8 mm distance from each other. At 700 μs, all of the initial matrix cracks are propagated to delamination at lower interface.

2.4.2 Computational Results

Finite element analyses are conducted with Christensen failure criterion to correlate crack location and sequence with experiments. Resulting matrix crack initiation and propagation schemes of $[0_7/90_4]$ and $[90_7/0_4]_s$ configurations are presented in Fig. 2.10a and b respectively.

In $[0_7/90_4]_s$ stacking sequence, represented in Fig. 2.10a, local matrix damage is predicted at the impact location, unlike experimental results that produced no visible surface damage. However at the side section, a similar crack pattern is obtained. Initially, a matrix crack is initiated at bottom close to the center and after 8 μs, it propagated towards the center diagonally reaching to the upper interface. Afterwards, matrix cracking propagated just below and above interfaces resembling a

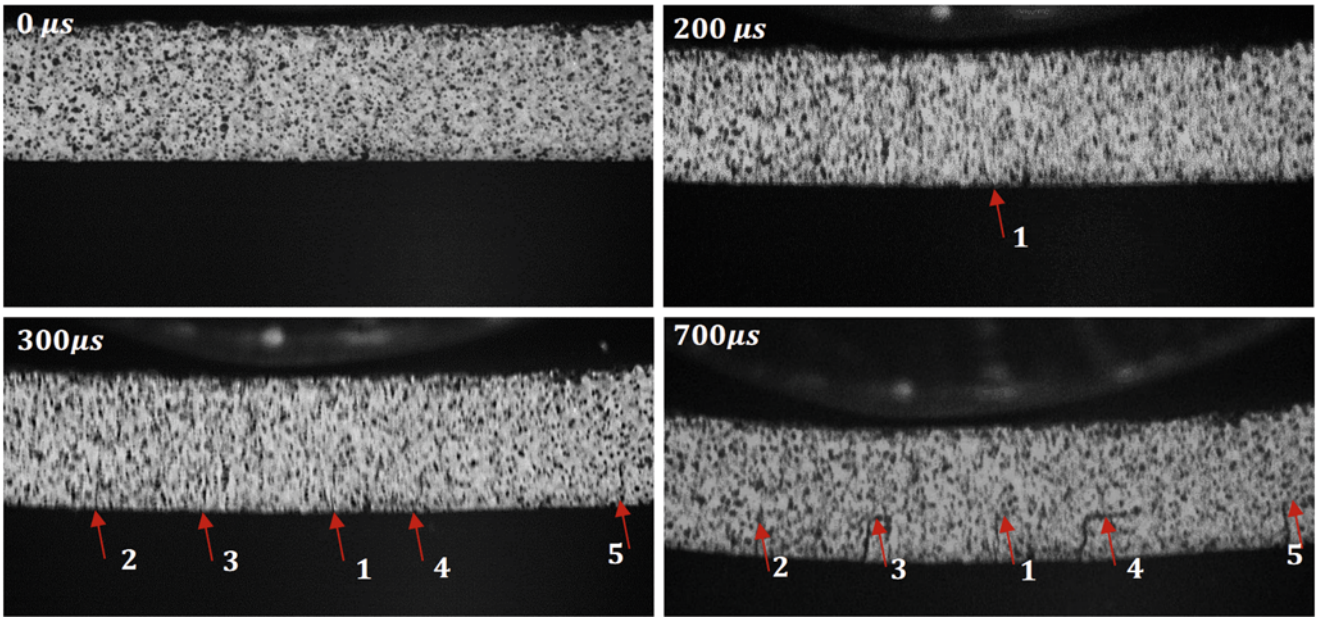

Fig. 2.9 High speed camera images of $[90_7/0_4]_s$ specimen taken in 20,000 fps showing matrix cracking initiation and propagation to delamination

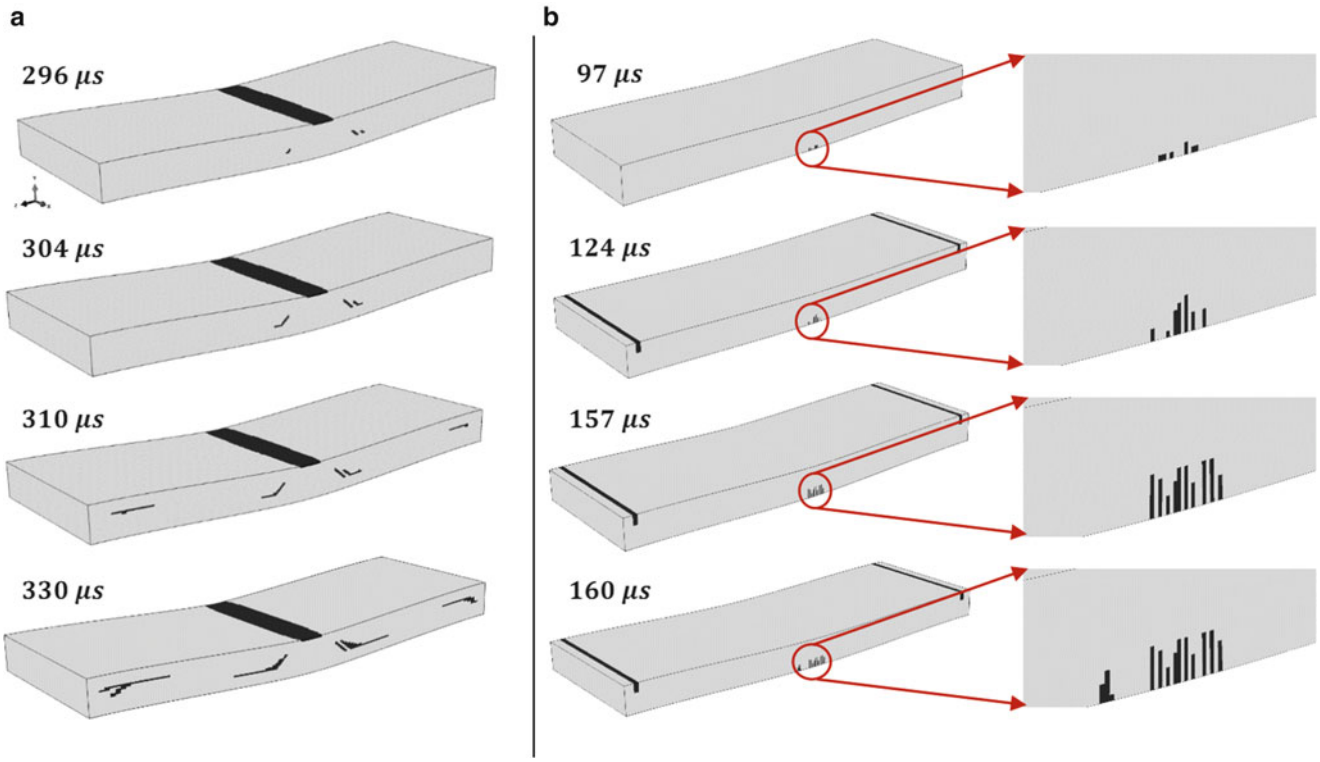

Fig. 2.10 Matrix crack initiation and progression scheme predicted by Christensen criterion for (**a**) $[0_7/90_4]_s$ and (**b**) $[90_7/0_4]_s$ stacking sequences

delamination pattern. While the crack angle of 45° is very close to the experiment results, the distance between two matrix cracks were about two times shorter than experimental results. In $[90_7/0_4]_s$ stacking sequence, represented in Fig. 2.10b, several matrix cracks are initiated in a region of 2 mm at bottom layer progressing perpendicular towards the bottom 0/90 interface. Upon reaching interface at 157 μs, additional matrix cracks are obtained due to lack of delamination damage in the computational model.

2.5 Conclusions

Experimental and computational studies are conducted on $[0_7/90_4]_s$ and $[90_7/0_4]_s$ 2-D beam-like unidirectional CFRP laminates to evaluate the failure progression of composites under out-of-plane impact loading. The line load impact tests on a composite plate was carried out to observe the impact failure phenomena from the edge using a high-speed camera and DIC system. Two different failure modes were captured depending on the stacking sequence. For $[0_7/90_4]_s$ lay-up, the damage initiates as delamination in the bottom interface followed by matrix cracking towards the impact point causing delamination in the upper layer. For $[90_7/0_4]_s$ lay-up, vertical matrix cracks initiate at the lower 90 layers in the line of impact, leading to delamination of the lower interface. Finite element simulations using Christensen matrix failure model was able to capture the general trend of matrix failure initiation and propagation observed in the experiments for both layups. A further study is being carried out to implement Cohesive Zone Method to model subsequent delamination observed in the experiments.

Acknowledgements The authors would like to acknowledge the contributions of METU Center for Wind Energy for allowing access to the experimental facilities. The authors would also like thank to Ayse Begum Erdem, Ali Gezer, and Miray Aydan Arca for their contributions.

References

1. Roeseler, B., Sarh, B., Kismarton, M.: Composite structures-the first 100 years. In: 16th International Conference on Composite Materials, Kyoto, 8–13 July 2007
2. Cantwell, W.J., Curtis, P.T., Morton, J.: An assessment of the impact performance of CFRP reinforced with high-strain carbon fibres. Compos. Sci. Technol. **25**, 133–148 (1986)
3. Choi, H.Y., Downs, R.J., Chang, F.-K.: A new approach toward understanding damage mechanisms and mechanics of laminated composites due to low-velocity impact: Part I—experiments. J. Compos. Mater. **25**, 992–1011 (1991)
4. Geubelle, P.H., Baylor, J.S.: Impact-induced delamination of composites: a 2D simulation. Compos. Part B **29**(5), 589–602 (1998)
5. Lopes, C.S., Seresta, O., Coquet, Y., Gürdal, Z., Camanho, P.P., Thuis, B.: Low-velocity impact damage on dispersed stacking sequence laminates. Part I: experiments. Compos. Sci. Technol. **69**(7–8), 926–936 (2009)
6. Lopes, C.S., Camanho, P.P., Gürdal, Z., Maimí, P., González, E.V.: Low-velocity impact damage on dispersed stacking sequence laminates. Part II: numerical simulations. Compos. Sci. Technol. **69**(7–8), 937–947 (2009)
7. Christensen, R.M.: The numbers of elastic properties and failure parameters for fiber composites. J. Eng. Mater. Technol. **120**(2), 110–113 (1998)
8. Hiel, C.C., Sumich, M., Chappell, D.P.: A curved beam test specimen for determining the interlaminar tensile strength of a laminated composite. J. Compos. Mater. **25**, 854–868 (1991)
9. Cheremisinoff, N.P. (ed.): Handbook of Ceramics and Composites: Mechanical Properties and Specialty Applications, p. 528. CRC Press, New York (1991)
10. Shi, Y., Pinna, C., Soutis, C.: Modelling impact damage in composite laminates: a simulation of intra- and inter-laminar cracking. Compos. Struct. **114**, 10–19 (2014)